Key Engineering Materials
ISSN: 1662-9795, Vol. 988, pp 47-62
doi:10.4028/p-gNXRC5
© 2024 The Author(s). Published by Trans Tech Publications Ltd, Switzerland.
Submitted: 2023-11-22
Revised: 2024-03-05
Accepted: 2024-04-08
Online: 2024-09-27

Extrusion Benchmark 2023: Effect of Die Design on Profile Speed, Seam Weld Quality and Microstructure of Hollow Tubes

Riccardo Pelaccia[1,a*], Marco Negozio[2,b], Sara Di Donato[2,c], Barbara Reggiani[1,3,d], Lorenzo Donati[2,e]

[1]DISMI Department of Sciences and Methods for Engineering, University of Modena and Reggio Emilia, Via Amendola 2, 42122, Reggio Emilia, Italy

[2]DIN Department of Industrial Engineering, University of Bologna, Viale Risorgimento 2, 40136, Bologna, Italy

[3]INTERMECH, University of Modena and Reggio Emilia, Italy

[a*]riccardo.pelaccia@unimore.it, [b]marco.negozio2@unibo.it, [c]sara.didonato2@unibo.it, [d]barbara.reggiani@unimore.it, [e]l.donati@unibo.it

Keywords: Extrusion benchmark, AA6082, process monitoring, charge welds, seam welds, microstructure, simulation validation.

Abstract. The Extrusion Benchmark 2023 was focused on the evaluation of different die design strategies for the manufacturing of AA6082 hollow tubes (40 mm external diameter and 4 mm thickness) through a porthole die with 3 openings. The extrusion process was monitored in industrial environment in terms of press load, profiles' speed, profiles' exit temperature, and die temperatures under different processing conditions (air quenching, water quenching, nitrogen die cooling). Extruded profiles were then analyzed in terms of seam weld quality, charge weld extension and microstructure evolution for both air/water quench and the presence/absence of nitrogen cooling. The results of the study are aimed at validating FEM simulation outputs in the context of the International Conference on Extrusion and Benchmark (ICEB).

Introduction

Over the years, the FEM numerical simulation has become a powerful tool for die makers and, more recently, for extruders in order to investigate the die design and the process parameters effects in the extrusion of aluminum profiles. In order to provide to Extrusion Industry a place to discuss numerical techniques and to train users in FEM simulation, the 'ICEB - International Conference on Extrusion and Benchmark conference series was settled [1]. The aim of the conference is to merge the typical conference format with a benchmark session where participants are asked to analyze a specific extrusion problem whose results are disclosed to participants only during conference days. The Extrusion Benchmark is a quadrennial event where experts in the field of aluminum extrusion and FEM analysis join together to verify the progress of the performance and accuracy of FEM simulations for process optimization and to share knowledge advancements in the field. Within the benchmark session, in order to provide an even point of comparison between experiments and simulations, it is extremely important that experimental trials provide clear indications of critical aspects of the process. For these reasons, a different die is designed at every benchmark: in 2007 the focus was on pocket design [2]; in 2009 it was on the influence of tongue deflection in U-shape profiles [3]; in 2011 different strategies for port-hole balancing were used for hollow profiles extrusion [4] [5]; in 2013 the experimental investigations were aimed at predicting the effects of mandrel deflection [6]; in 2015 the effect of bearing shape (straight, chocked or relieved) and length was investigated [7] [8] while in 2017 the die was designed in order to allow mandrels shift during the process to verify the effects on the profiles [9].

This paper summarizes information in terms of simulation settings and output results related to the Extrusion Benchmark 2023. The benchmark was focused on the extrusion of 3 hollow tubes (40 mm external diameter and 4mm thickness) with EN AW-6082 alloy. The die was designed and

This article is an open access article under the terms and conditions of the Creative Commons Attribution (CC BY) license (https://creativecommons.org/licenses/by/4.0)

manufactured by Almax Mori (Rovereto, TN) with different features (i.e. cylindrical or conical ports, bearing lengths, and radii) for each of the 3 openings to attain different metal flows (and consequently different strains, strain rates and temperatures) in the tubes. The trials were performed at the Metra plant in Rodengo Saiano (Brescia, IT) on a 40MN press; thermal field was monitored by means of a contactless pyrometer on a profile (profile 1) and eleven thermo-sensors were inserted in the die, in the die ring and the backer. The backer was characterized by a specific channel for nitrogen flowing aimed at investigating cooling effects. Several extrusion data were continuously acquired by the control system of the press including the puller speed and force and the extrusion load. After the extrusion trials, the profiles were analyzed at the University of Bologna in order to determine the position and quality of the seam welds, the extent of the charge welds, and the microstructure in the profiles cross-section under air or water quench and with/without nitrogen cooling.

Simulation Settings

In this section, all the information provided to the benchmark participants for running the analysis of the Extrusion Benchmark 2023 is reported. The benchmark campaign (Fig. 1) involved the extrusion of fifteen AA6082 billets by varying the nitrogen flow rate (0% or 100% valve opening) and the quenching conditions (only air or water/air spray). The first 3 billets were used to warm up the system (billets 1 to 3) and to approximate a 'steady state' thermal condition. Then, 2 more billets (billets 4 and 5) were extruded in the same conditions thus representing the benchmark trials with repetitions. The subsequent ten billets were extruded to analyze the efficiency of the nitrogen cooling and the effect of water quenching on the microstructure evolution of the extrudates. A ram speed of 4.4 mm/s was used for all the trials; a ram stroke of 650 mm was set over a billet length of 680 mm (thus meaning 30 mm of rest length) and a puller tensile force of 350kg (3500N) was applied. In detail, Tab. 1 summarizes the process parameters necessary for the simulation setting.

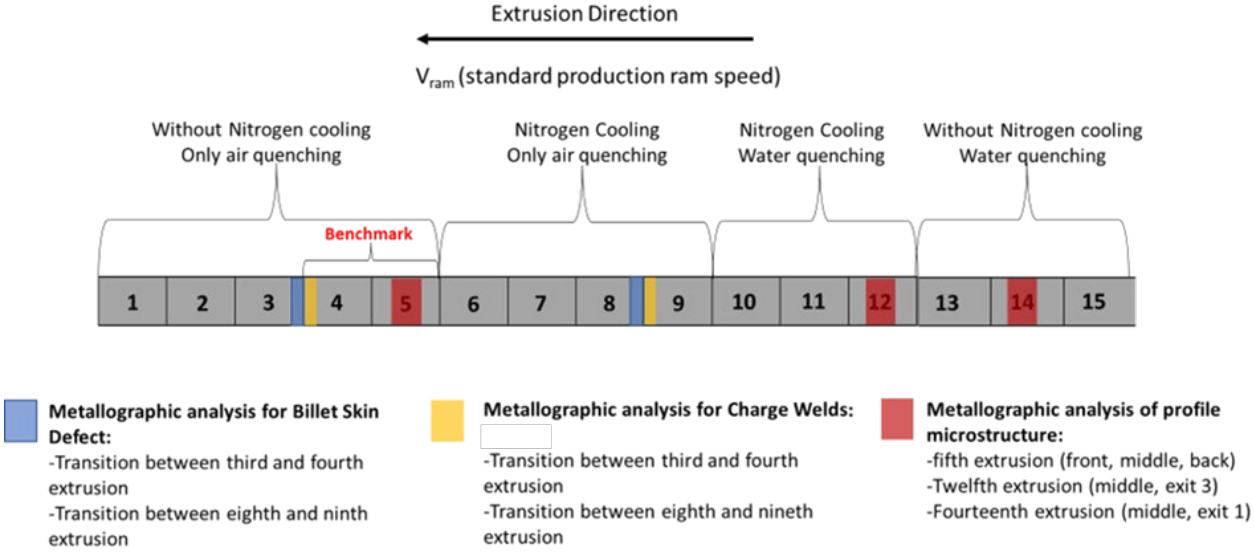

Fig. 1. Selected Design of Experiment (DOE) for the Extrusion Benchmark 2023: Fifteen billets were extruded by varying the nitrogen cooling and the quenching parameters.

As reported in Fig. 1, some profiles were selected for the 'front and back-end defects' evaluation and microstructure analysis:

- Transition between the third and the fourth billets for the evaluation of both skin defect and charge weld extent.
- Transition between the eighth and the ninth billets for the evaluation of both skin defect and charge welds extent.
- Fifth billet (all profiles: middle positions with respect to the extrusion direction) for the metallographic analysis of the profile microstructure using only air quenching.

- Twelfth billet (profile 3: middle position with respect to the extrusion direction) for the metallographic analysis of the profile microstructure using both water quenching and nitrogen cooling.
- Fourteenth billet (profile 1: middle position with respect to the extrusion direction) for the metallographic analysis of the profile microstructure using water quenching without nitrogen cooling.

Table 1. Process Parameters.

Process Parameter	Value
Profile alloy	AA6082
Billet diameter	279 [mm]
Container diameter	286 [mm]
Billet length	680 [mm]
Billet rest	30 [mm]
Skin layer thickness	0.3 [mm]
Ram speed -all tested conditions-	4.4 [mm/s]
Max press load	4000 [ton]/40 [MN]
Ram Temperature	350 [°C]
Container Temperature	390-425 [°C] (ram-die)
Pre-heating Billet Temperature	440 [°C] (no taper)
Pre-heating Die Temperature	480 [°C]
Nitrogen Inlet Temperature	-196 [°C]
Nitrogen Inlet Pressure	3 [bars]
Nitrogen Inlet Tube Diameter (internal)	5,5 [mm]

Geometries. A porthole die with 3 tube-shaped openings for hollow profiles extrusion was used for the benchmark trials. The die assembly (AISI H-13 steel, tempered 45-47 HRC) was composed of five parts: the mandrel, the die, the die ring, the backer, and the bolster (Fig. 2 and Fig. 3). Geometries CAD files can be asked to benchmark organizers (iceb.din@unibo.it). The final (cold) profile had an external diameter of 40 mm and a thickness of 4 mm, so the area of the single profile surface was 452.16 mm^2 thus leading to a total profiles area of 1356.48 mm^2. The material flow within the tooling set was different for the 3 profiles (Fig. 4) with the aim to generate high velocity deviations at the exit, phenomena to be captured with the numerical simulation:

- Exit N°1: Conical ports and cylindrical bearings. Bearings on the die surface had an inlet fillet radius of 1 mm and 6 mm in length, while the bearings on the mandrel surface had the same length without the fillet radius.
- Exit N°2: Cylindrical ports and cylindrical bearings. Bearings on the die surface had an inlet fillet radius of 1 mm and 7 mm in length, while the bearings on the mandrel surface had the same length without the fillet radius.
- Exit N°3: Conical ports and tapered bearings. Bearings on the die surface had an inlet fillet radius of 1mm, a choke (angle of 1°, length of 4 mm) and a final cylindrical part 1 mm length. The bearings on the mandrel surface were 5 mm length.

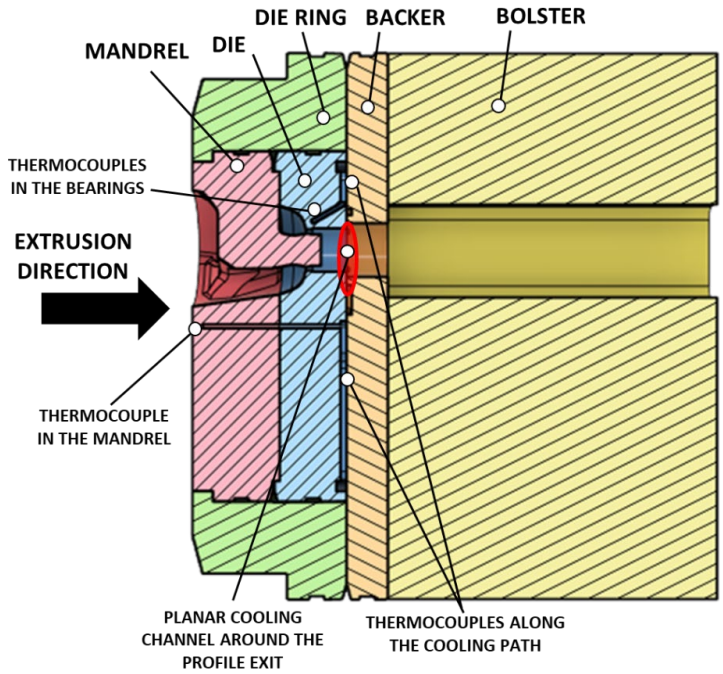

Fig. 2. Die assembly with die ring, backer and bolster.

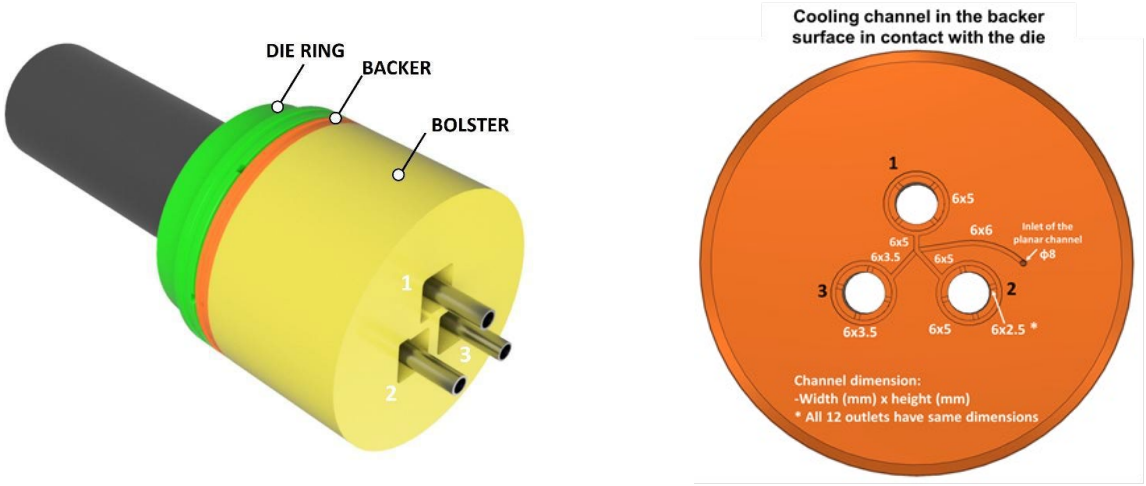

Fig. 3. Rendering of the billet and tools set-up (left) and Cooling Channel Design (right).

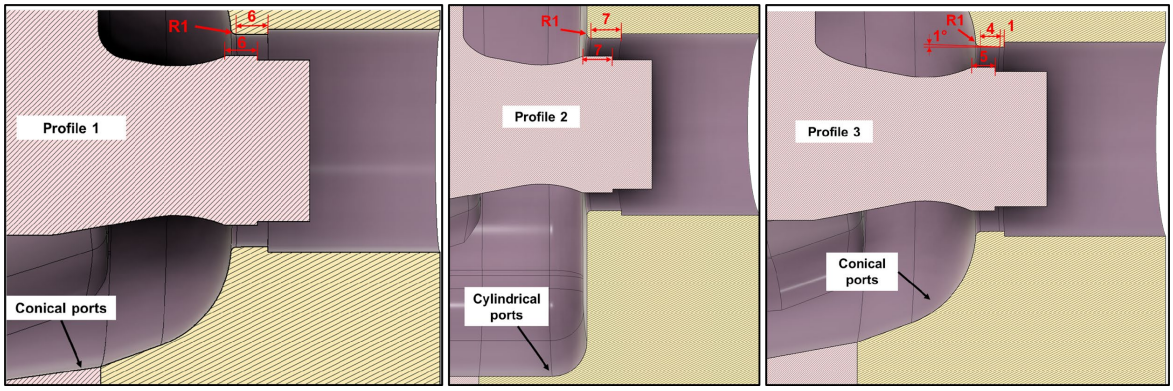

Fig. 4. Bearings main dimensions.

The experimental trials involved the use of nitrogen cooling for some final tested conditions: the cooling channel was manufactured in the backer surface in contact with the die. In detail, Fig. 3b shows the cooling path and the channel dimensions. One of the main aim of 2023 Benchmark was to investigate the evolution of the thermal field during the extrusion process in both uncooled and cooled conditions, making a deeper monitoring of the thermal behavior of tools by means of several thermocouples necessary.

In detail, eleven thermocouples were used for monitoring the thermal evolution of the die/tools system (Fig. 5): thermocouples from T1 to T6 were placed on the surface in contact with the backer to follow the thermal field evolution along the nitrogen cooling path, from T7 to T9 were positioned near the bearing region, T10 in the mandrel and T11 in contact with the die ring. In addition, a contactless pyrometer was used for the monitoring of the profile 1 temperature at a distance of 1500 mm from the bolster surface (Fig. 6). Fig. 6 also shows the position of the quenching zones: air quenching was always turned on during the trials while water quenching was used only in trials from 10 to 15 in order to analyze the effects in terms of microstructure evolution of the profiles. As quenching rates for air/water, it was suggested to participants to use their own data if available; otherwise, the following data were suggested: for air quenching, a decrease of profile temperature of 1°C/sec, while for water quenching of 100°C/sec.

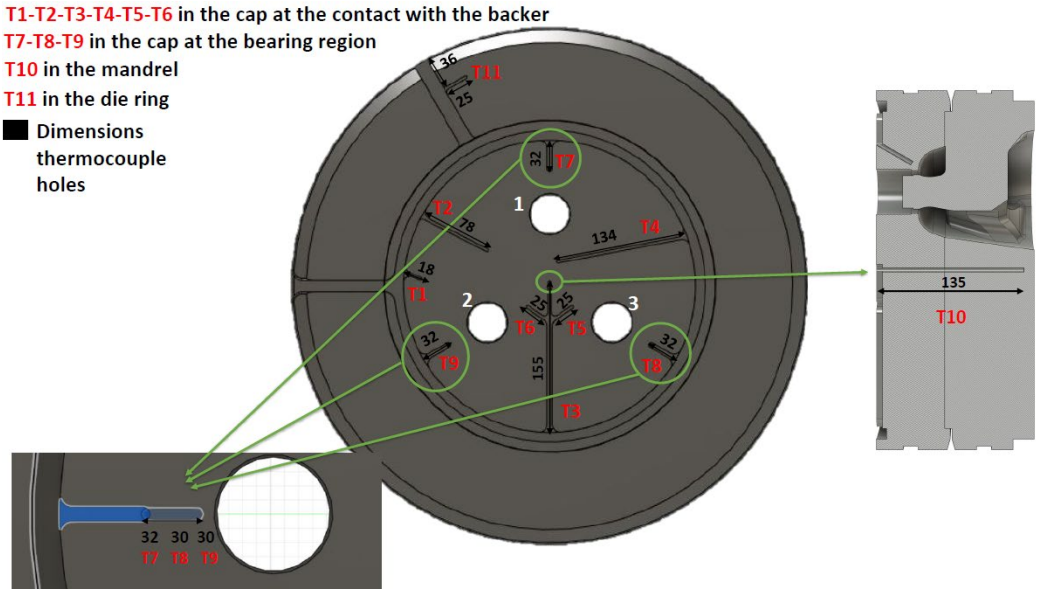

Fig. 5. Thermocouple positions (T1 to T11).

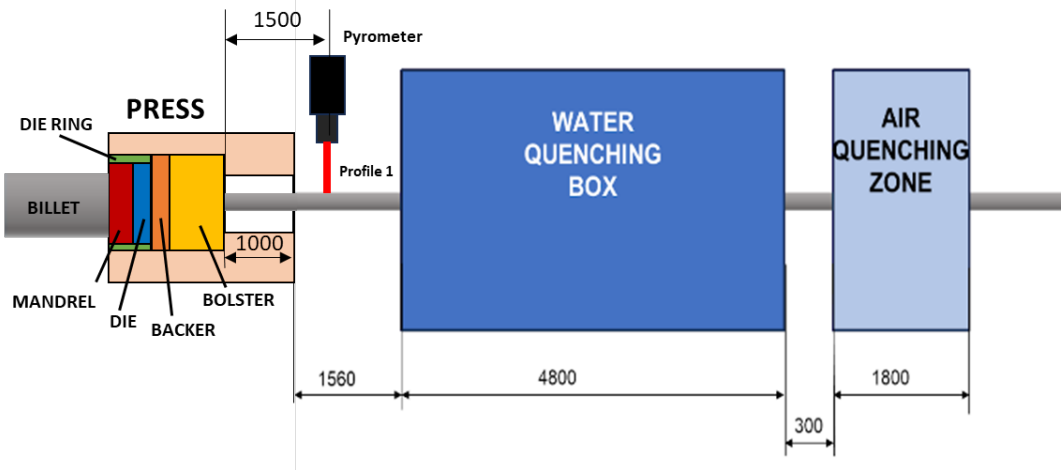

Fig. 6. Position of profile pyrometer spot and of quenching zones.

Billet flow stress. The AA6082 alloy was used for this edition of the Benchmark trials. Microstructure analysis and mechanical characterization of the alloy were carried out at the Department of Industrial Engineering of the University of Bologna. The material flow stress characterization was performed by means of hot torsion tests on homogenized alloy samples. Tests were performed with equivalent strain rates of 0.01, 0.1, 1, and 10 s^{-1}, in the temperature range from 440 to 550 °C (from 713.15 to 823.15 K) and the results presented in terms of equivalent stress ($\bar{\sigma}$) vs equivalent strain ($\bar{\varepsilon}$). Details of the experiment can be found in the reference paper [10]. The material flow stress curves were furthermore regressed by the Hensel-Spittel and the Hyperbolic sine models. The Hensel-Spittel law [11] for the prediction of the material flow stress is reported in eq. 1:

$$\bar{\sigma} = A\, e^{m_1 T} \bar{\varepsilon}^{m_2} \dot{\bar{\varepsilon}}^{m_3} e^{\frac{m_4}{\bar{\varepsilon}}} (1+\bar{\varepsilon})^{m_5 T} e^{m_7 \bar{\varepsilon}} \dot{\bar{\varepsilon}}^{m_8 T} T^{m_9} \quad (1)$$

Regression of the flow stress data can be performed with all the 9 regression coefficients (A and m_1 to m_9) or with only a part of them: below correlations with 5,6,7,8 and 9 coefficients are proposed for temperature expressed in K (Tab. 2) and °C (Tab. 3).

Table 2. Hensel-Spittel coefficients with temperature expressed in K (Temperature range validity 713-823 K).

Parameters	5 parameters	6 parameters	7 parameters	8 parameters	9 parameters
A [MPa]	182.562	176.285	178.685	182.161	87.963
m1 [K^{-1}]	-0.0022426	-0.0023064	-0.0023004	-0.00215	-0.0035864
m2	-0.0405691	-0.0610555	-0.0542036	0.008047	0.0081011
m3	0.105639	0.1052751	0.1062478	-0.02175	-0.0225208
m4	-0.0012775	-0.0012881	-0.00121413	-0.00029	-0.00029223
m5 [K^{-1}]	0	7.54071E-05	5.60459E-05	-7.2E-05	-7.215E-05
m7	0	0	-0.0003077	0.000282	0.0002987
m8 [K^{-1}]	0	0	0	0.000142	0.0001588
m9	0	0	0	0	0.2766873
R2	0.972	0.960	0.965	0.969	0.939

Table 3. Hensel-Spittel coefficients with temperature expressed in °C (Temperature range validity 440-550 °C).

Parameters	5 parameters	6 parameters	7 parameters	8 parameters	9 parameters
A [MPa]	98.851	96.259	107.028	99.774	99.722
m1 [K^{-1}]	-0.0022408	-0.0023101	-0.0022578	-0.00212	-0.00212
m2	-0.0405691	-0.0550745	0.0074409	0.007399	0.007401
m3	0.105639	0.105639	0.0880616	0.017222	0.017216
m4	-0.0012775	-0.00128502	-0.0002925	-0.00029	-0.00029
m5 [K^{-1}]	0	0.00009201	-0.00010522	-0.0001	-0.0001
m7	0	0	6.43551E-05	2.35E-05	2.37E-05
m8 [K^{-1}]	0	0	0	0.000142	0.000142
m9	0	0	0	0	9.33E-05
R2	0.972	0.965	0.970	0.968	0.968

The eq. 2 describes the Hyperbolic sine model proposed by Garofalo [12] where R is the universal gas constant (8.314 J/mol*K), Q is the apparent activation energy for plastic flow, A, α and n are material constants. The material parameters for temperature expressed in Kelvin are reported in Tab. 4

$$\bar{\sigma} = \frac{1}{a}\sinh^{-1}\left[\left[\frac{1}{A}\dot{\varepsilon}\exp\left(\frac{Q}{RT}\right)\right]^{\frac{1}{n}}\right] = \frac{1}{a}\sinh^{-1}\left[\left(\frac{Z}{A}\right)^{\frac{1}{n}}\right] \quad (2)$$

Table 4. Sin-hyperbolic model parameters.

Q [J/mol]	A [s^{-1}]	α [MPa^{-1}]	n
1.036E+05	7.95 E+04	0.045	5.499

Microstructural analyses of the tested billet were carried out to measure the initial grain shape and dimension. Fig. 7 reports the longitudinal and transversal section of a specimen extracted from the AA6082-O logs used for the trials. It is possible to observe that grains are almost spherical (equi-

axials) with an average diameter of 112 μm in the longitudinal direction and 118 μm in the transverse direction. The measurements were carried out according to the intercept method ASTM E 112-13. The acquired billet skin thickness was equal to 0.3 mm as reported also in Tab. 1.

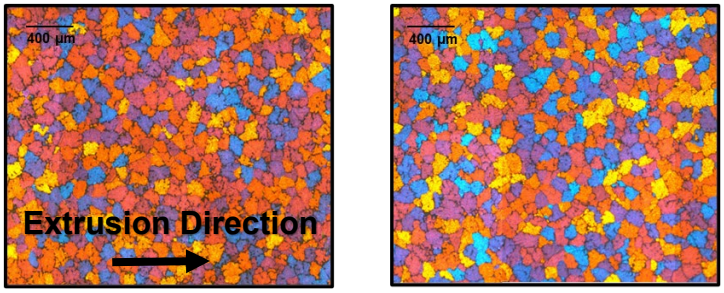

Fig. 7. Microstructural analyses of AA-6082 specimen extracted from tested billets (after polishing, electrolytic etching with Barker reagent and analysis with polarized light). Left longitudinal section of the billet (extrusion direction left to right); right transversal section (extrusion direction out of image plane).

Thermal field, Heat exchange and friction. The porthole die was pre-heated in oven at 480°C. Then, during the die loading into the press, the temperature in the monitored locations decreased for the heat exchange to the "cold parts" of the press. For benchmark participants, the temperatures in all locations, before the first extrusion and before the fourth one (steady state uncooled condition), were an input, thus allowing to select different simulation strategies: transient simulations from the first run to reach the steady state condition, or steady state analysis of the runs selected for the experimental-numerical comparison. All the data on thermocouples' temperature are reported in Tab. 5 and Tab. 7, while the results are deeply discussed in the "experimental results" section.

Table 5. Initial Temperatures.

Ram		350 [°C]
Container		390-425 [°C] (ram-die)
Billet	Billet pre-heating temperature	440 [°C] (no taper)
Die	Die pre-heating oven (mandrel, die, backer and die-ring)	480°C
	At beginning of trials (before extruding **billet 1**).	Point T1: 445 [°C] Point T2: 457 [°C] Point T3: 457 [°C] Point T4: 440 [°C] Point T5: 458 [°C] Point T6: 458 [°C] Point T7: 473 [°C] Point T8: 468 [°C] Point T9: 471 [°C] Point T10: 476 [°C] Point T11: 442 [°C]
	Before extruding **billet 4 (benchmark reference test)**.	Point T1: 359 [°C] Point T2: 400 [°C] Point T3: 428 [°C] Point T4: 429 [°C] Point T5: 432 [°C] Point T6: 436 [°C] Point T7: 468 [°C] Point T8: 441 [°C] Point T9: 483 [°C] Point T10: 526 [°C] Point T11: 306 [°C]

Heat exchange models may significantly vary within different numerical codes. However, based on the state of art [13] [14] and on the authors' knowledge, data in terms of heat exchange and nitrogen properties (Tab. 6) were provided to the participants, if code's database parameters were not available.

Table 6. Materials Heat Exchanges.

Aluminum		
Conductivity	210	[N/(s·°C)]
Heat capacity	2,94	[N/(mm^2·°C)]
Steel (AISI H-13)		
Conductivity	24,33	[N/(s·°C)]
Heat capacity	4,63	[N/(mm^2·°C)]
Aluminum-Steel		
Heat exchange	11	[N/(s mm·°C)]
Nitrogen (-196°C at room pressure)		
Physical Properties	Liquid Nitrogen	Gas Nitrogen
Density [kg/m^3]	806.59	4.56
Dynamic Viscosity [Pa·s]	1.61E-04	5.43E-06
Heat capacity at constant pressure [J/(Kg·K)]	2041	1123
Thermal conductivity [W/(m·K)]	0.14605	7E-03

Concerning the simulation of nitrogen cooling, the assumption that only liquid nitrogen flowed within the cooling path could lead to an overestimate of the cooling efficiency, while an underestimation could be obtained by selecting a fully gaseous model. The use of a homogenous fluid approach [15] was suggested to benchmark participants, considering the liquid-gas mixture as a single fluid with pseudo properties.

Friction of aluminum on steel at extrusion temperatures is usually computed as complete sticking, except in bearing zones where some sliding may occur [14]. Commonly, the following shear friction model is implemented:

$$\tau = m \cdot \tau_s \tag{3}$$

with τ being the shear friction stress, τ_s the material shear stress, and m the friction factor that is equal to 1 in the fully sticking condition.

Experimental Results

Thermal field. Fig. 8 shows the thermal and load histories of the whole experimental campaign: the temperatures acquired by the thermocouples and by the pyrometer, as well as the extrusion load, were reported in the graph. The porthole die was pre-heated in oven at 480°C then, during the die loading, the temperature in the monitored locations decreased to 445-476°C as shown in Tab. 7. In detail, temperatures in the backer (from T1 to T6 along the cooling path, T11 in contact with the die ring) reached values of about 445°C as a result of the contact with the cold parts of the press. In proximity to the bearings (T7, T8, T9) and within the mandrel (T10), the decrease in temperature was less pronounced with the minimum value of 468°C recorded in T8. During the first extrusion, the ram speed was lower, and the ram was also stopped to allow the puller to engage the profiles; all thermocouples, except T10, continued to record a decrease in temperature for the heat exchange with the press. At the beginning of the second extrusion, the ram speed was set to 4.4 mm/s and the heat generated by the aluminum under deformation increased: the thermocouples T4-T6 nearby the profiles' exit recorded a maximum value of about 450 °C, T1 and T2 nearby the inlet channel marked 370°C and 416°C respectively, T9 (bearings exit 2) indicated the value of 480 °C, T8 (bearings exit 3) only 441 °C, while T7 (bearings exit 1) recorded an intermediate value of 465 °C. As expected, the highest temperature of 520 °C was observed in T10 (mandrel) and the lowest one at about 330°C

in T11 (die ring). Indeed, as a consequence of manufacturing issues of the holes, T7-T9 locations were not close enough to capture the real bearings temperature that should be very similar to the profile temperature (547 °C). In addition, T8 temperature was unexpectedly low if compared to T7 since profiles 1 and 3 had the same velocity (Fig. 9). Therefore, during the die loading, T8 had probably moved from its seat.

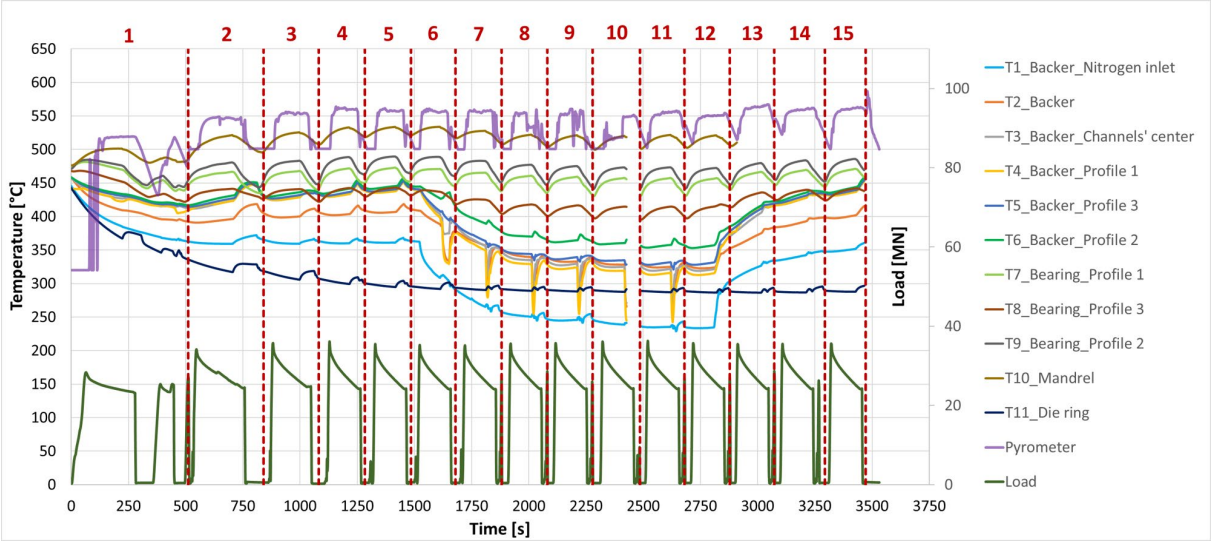

Fig. 8. Thermal and load history of the whole experimental campaign. (15 billets).

Table 7. Thermocouples' recordings.

Thermocouples' Temperature [°C]											
	T1	**T2**	**T3**	**T4**	**T5**	**T6**	**T7**	**T8**	**T9**	**T10**	**T11**
Before Extrusion 1	445	457	457	440	458	458	473	468	471	476	442
Before Extrusion 4	359	400	428	429	432	436	468	441	483	526	306
Extrusion 5	361	406	437	437	441	444	473	445	490	535	295
Extrusion 12	234	323	320	320	330	360	463	417	471	520	286

During the following two runs, the temperatures generally rose, while the difference between the values of the fourth and fifth extrusion was negligible, thus evidencing the achievement of the steady state uncooled condition (Tab. 7). For the fifth extrusion, T10 (mandrel) recorded a value of 535°C (15 °C more than the second extrusion), T7 (bearings exit 1), T8 (bearings exit 3) and T9 (bearings exit 2) acquired 473°C, 445 °C and 490°C respectively, against 465°C, 441°C and 480°C of the second extrusion. Except for T11 (die ring), which showed a temperature of 295°C (35 °C lower than the second extrusion), the temperature in the backer remained more stable, evidencing differences below 5 °C with respect to the second run. The pyrometer registered a maximum temperature of 560°C for profile 1 (13°C more than the second extrusion).

During the sixth extrusion, the nitrogen valve was fully opened until the end of the twelfth run. The nitrogen valve remained opened also during the billet change in order to achieve a liquid nitrogen flow in the channel instead of gas nitrogen or a mixture [15], and to promote the achievement of the steady state condition in a few runs. The acquisition system crushed for some seconds during the tenth extrusion thus generating the lack of data at around 2400 seconds.

Analyzing the temperature evolution of T1 located nearby the nitrogen inlet, it is worth noting that the steady state condition was reached during the last extrusion with the nitrogen cooling, where the T1 temperature, after a significant decrease during the previous runs, remained constant at the value of 234°C. In detail, the temperature at T1 exhibited a rapid decrease during the first two runs (6th and 7th), dropping from 365°C to 265°C. Subsequently, the thermal gradient decreased, reaching a

steady-state value of 234°C after additional five billets. The other thermocouples in the backer showed a comparable behavior; however, it is worth noting the limits of the selected channel design: T6 located nearby the exit 2 recorded temperatures (360°C during the 12th run) about 40°C higher than T3 and T4 (320°C during the 12th run) positioned at the center of the channel, evidencing the unbalanced distribution of the nitrogen flow. The channel design promoted the nitrogen flow towards the exit of the profile 3 (T5 with a minimum value of 330°) and made much less effective the cooling around the other exits. This trend was confirmed also by the bearings temperatures, where the higher cooling effect was captured by T8 (exit 3, from 445 °C to 417 °C), while the lower one by T7 (exit 1, from 475°C to 463°C). The decrease in temperature registered by T10 (mandrel, from 535°C to 520°C) was not caused by the nitrogen since the cooling channel was too far from the mandrel [15]. During the last three extrusions, the nitrogen cooling was turned off and the temperatures generally rose, thus achieving comparable values between the last run and the steady state uncooled condition.

From the results discussion it is clear that, in this case, the cooling efficiency on the bearings surface was limited with a sole 10°C of change on the profiles exit temperature (from 560°C to 550°C for profile 1). According to the state of art [13] [15], the experimental campaign showed the potentiality of the nitrogen cooling, but also the wide margins of improvement of the channels if designed with the support of advanced numerical tools.

Extrusion Load. In term of extrusion load, a peak value of about 36 MN, over the 40 MN available, was registered and, as expected [15], the increase caused by the localized nitrogen cooling was negligible.

Profiles speed. Fig. 9 shows the velocity evolution of the profiles during the fourth extrusion (run selected for the benchmark analysis). During the first extrusion, before the use of the puller, the velocity of the profile 2 was qualitatively 50% higher than the ones of the other two profiles. Then, despite the application of a tensile force of 3500 N, the profile 2 continued to flow through the puller at a higher speed. In Fig. 9 the velocity of the profiles 1 and 3 was imposed by the puller (average speed of 195 mm/s), while the profile 2 (average speed of 225 mm/s, 15% higher than the puller one) was calculated by analysing the difference in terms of extrudates length at the end of the extrusion. The significant variations in profile speed are related to the variations in the geometries of the ports and bearings for the three profiles (Fig. 4).

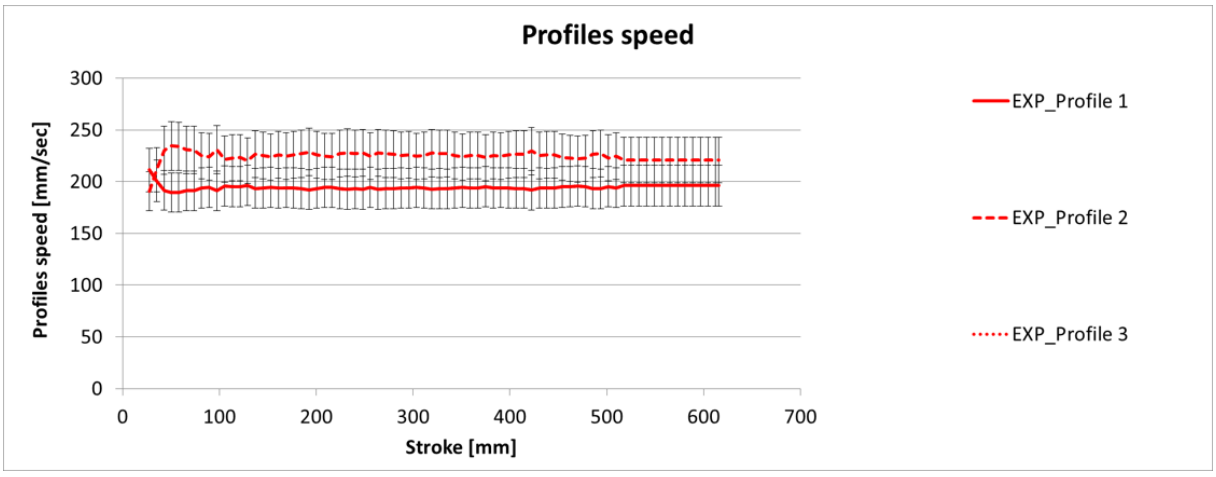

Fig. 9. Profiles speed (Billet 4).

In the present experimental campaign, contrary to the normal industrial practice that foresees the design of symmetrical geometries for multiple profiles, significant geometrical differences were voluntarily induced in the design of the ports and bearings of the 3 profiles with the aim to test the forecasting performance of numerical tools. Among them, profile 2 with cylindrical ports and cylindrical bearings resulted the faster one, while profile 3 with conical ports and choke was the slowest one. The cylindrical ports (profile 2) always guaranteed a faster material flow with respect to the conical ones (profiles 1,3), underlining that the effect of port geometry was more significant than that of the bearings in terms of speed changes. On one side, this was proved by the experimental

evidence that the speed difference between profile 3 and profile 1 (both extruded with conical ports) was not so high without the puller and negligible with the puller, despite the differences in the bearings configuration (choke for profile 3, 1 mm higher bearings length for profile 1). On the other side, despite the 1 mm higher bearings length of profile 2 with respect to profile 1, the former flowed faster due to the cylindrical ports. These results suggest the need to ponder the effects of all the involved geometric parameters and of their interactions for an optimized die and process design. Indeed, in this case, compensating for the speed differences generated by a conical port design does not appear to be an "easy task" using only the bearings optimization.

Charge welds and billet skin. Fig. 10a summarizes the terminology that will be used in this paragraph. It can be useful to remind that billet skin is usually found only when a short billet rest is used and it is related to the contamination of the profile by the outer layer of the billet (i.e. the billet skin), whose typical dimension is around of 0,2-0,4 mm, and accumulate at the billet end as a consequence of high sticking friction of aluminum on container. Billet skin contamination, when present, may start (BSS in Fig. 10a) before or after the stop mark and end (BSE) after it. Charge weld, instead, is related to the interaction between the old and the new billet in a continuous extrusion and its start (CWS) and end (CWE) are always located after the stop mark. Since the charge welds and the billet skin are deeply contaminated by oxides and impurities (thus leading to poor mechanical proprieties [10]), such portions (from BSS to CWE) have to be discarded and consequently the possibility of extent minimization is of relevant industrial interest.

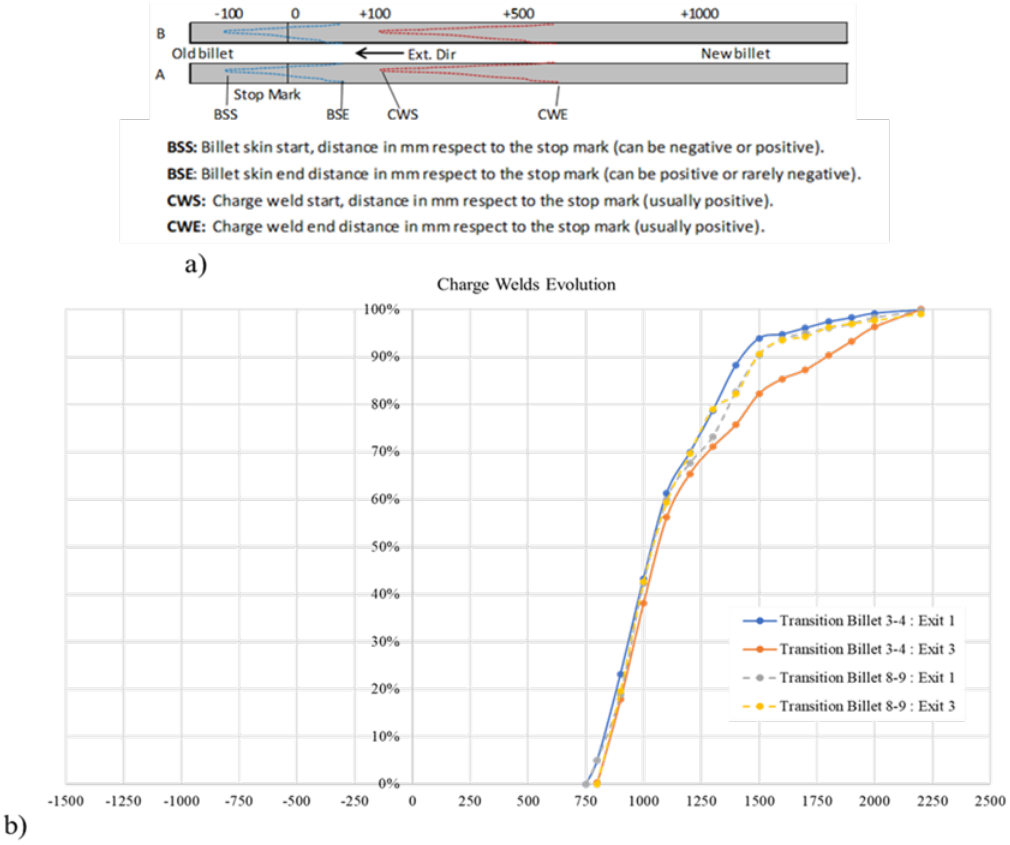

Fig. 10. Charge welds evolution for transitions between billets 3-4 and 8-9, Profiles 1-3.

All the analyzed profiles showed no evidence of billet skin contamination. Fig. 10b reports the evolution of charge welds in the transition between billets 3-4 and 8-9 for profiles 1 and 3. As evident from the graph depicted in the figure, the four patterns closely resemble each other, indicating an initial defect onset within the range of +750 to +800 mm from the stop mark, followed by a rapid expansion and extension of the defect in the range of +2100 to +2200 mm from the stop mark. In Fig. 11, an example of how the charge welds was calculated is reported. The process involved the etching of the profile, the acquisition and the analysis of the images.

The trend for the profile 2 was not reported in the present document due to the presence of the PCG (Peripheral Coarse Grain), which posed a significant challenge in precisely delineating the start and end points of the defect, as exemplified in Fig. 12, following the etching phase.

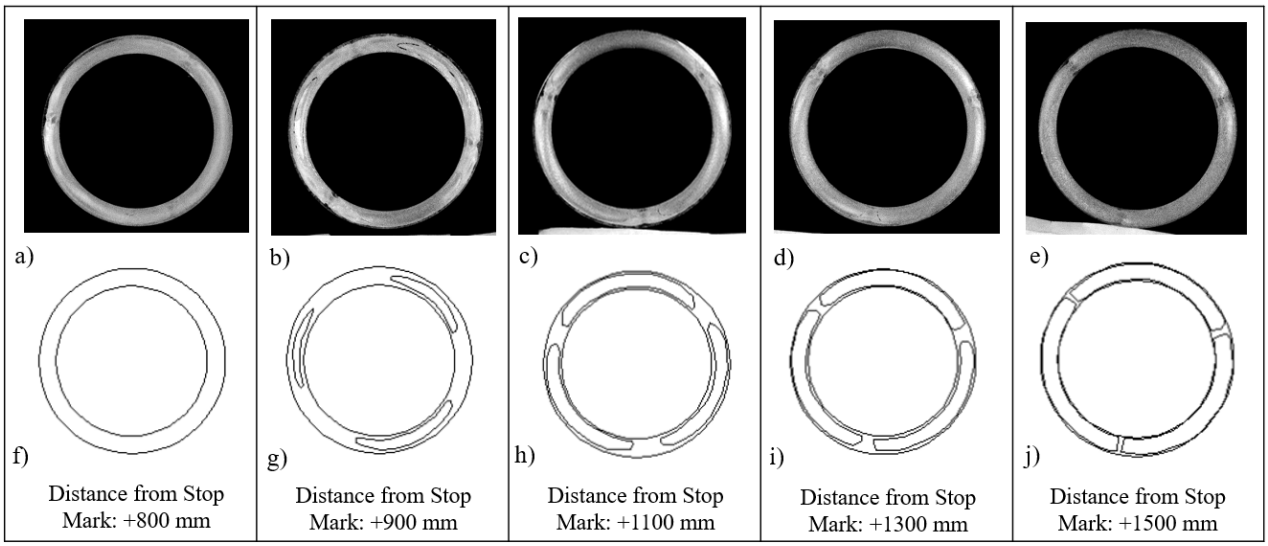

Fig. 11. Charge welds image analysis (Billet 3-4 transition, profile 3).

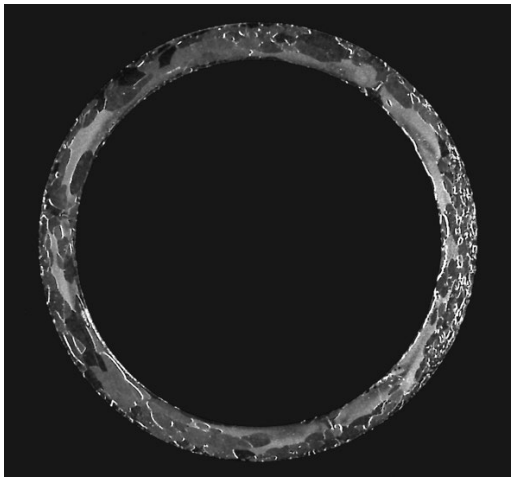

Fig. 12. Microstructure of the profile 2 in the billet 3-4 transition.

Microstructure. Specimens extracted from the middle of the extruded profiles were analyzed in terms of microstructure evolution. The image was acquired by using polarized light microscopy of the samples anodized (40 V dc, 4 min) with Barker's reagent (15 mL HBF4, 750 mL H2O). In order to properly discuss the obtained micrographs, it is important to remind that the billets had an average grain size of 112 μm on longitudinal direction and 118 μm on transverse direction. In Fig. 13, the microstructures of the profiles extruded from billet 5 with air quenching only and without nitrogen cooling are reported. The microstructure of profile 1 exhibits a fibrous grain structure with a thin PCG layer on the internal and external surfaces. In contrast, the microstructure of profile 2 differs from that of profile 1 due to a higher PCG thickness, both internally and externally (caused by the higher exit speed of the profile). Finally, profile 3 shows a completely fibrous microstructure. Measurements of grain sizes and PCG layers thicknesses are detailed in Tab. 8.

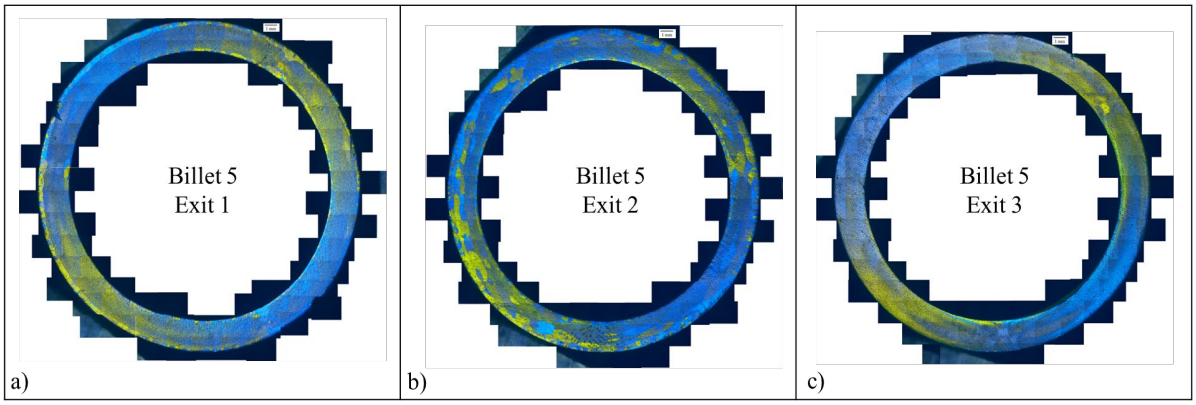

Fig. 13. Microstructure of profiles extruded from billet 5, middle of the extruded profiles: a) profile 1, b) profile 2, c) profile 3.

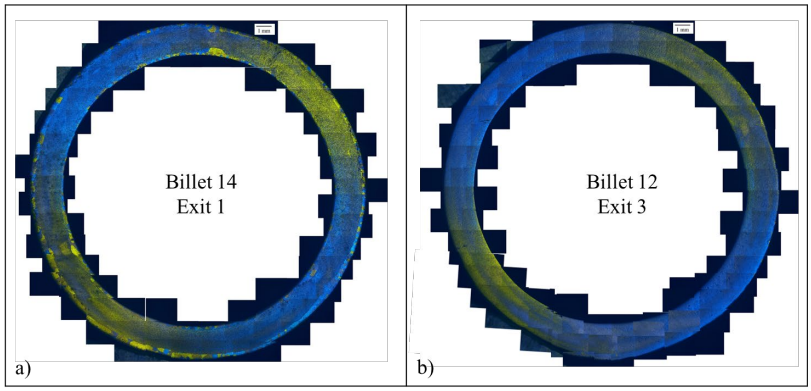

Fig. 14. Microstructure of the profiles extruded from a) Billet 14 profile 1, b) Billet 12 profile 3.

Table 8. Results of the PCG layer and grain size evaluation.

	Internal PCG layer [µm]	**External PCG Layer [µm]**	**Grain size range - Fibrous [µm]**	**Grain size range - PCG [µm]**
Billet 5 Exit 1	201	523	5-30	131-832
Billet 5 Exit 2	485	1154	5-30	142-1885
Billet 5 Exit 3	0	0	5-30	-
Billet 14 Exit 1	235	572	5-30	134-901
Billet 12 Exit 3	0	0	5-30	-

In Fig. 14, the microstructures of the profiles extruded from billet 14 (no nitrogen, water quenching, profile 1) (Fig. 14a) and billet 12 (nitrogen cooling, water quenching, profile 3) (Fig. 14b) are depicted. Notably, the microstructure in Fig. 14a closely resembles that in Fig. 13a (billet 5, profile 1), while the microstructure in Fig. 14b is completely fibrous as to the one in Fig. 13c (billet 5, profile 3). Stating these results, it is possible to understand that, in this case, the water quenching with air quenching generated a negligible effect on microstructure evolution with respect to the air quenching only. To measure the recrystallization layer on both the internal and external surfaces, 24 measurements were acquired (a measurement every 30° of the circumference on internal and external surfaces) and an average value was computed. Tab. 8 displays the values of recrystallized thickness in the analyzed cases, along with the corresponding range of grain sizes.

Seam weld quality. For the characterization of the seam weld quality, bulge tests were selected with respect to the conical expansion since they provide a higher accuracy and repeatability of the results [16]. Bulge tests were carried out on an Instron 250 kN press with a rubber plug of 29 mm in diameter that was compressed between two punches inside the tube with a constant ram speed of 0.5 mm/s. Plug pressure on the inside wall of the profile generated a biaxial tensile stress leading the tube to fracture in proximity of the seam welds. The two punches were constrained in order to displace in the longitudinal direction only and the movement was assigned to the upper one (Fig. 15a).

Following [18], a specimen length of 145mm was selected in order to avoid any influence on the results. A uniform deformation in the rubber plug and the absence of any buckling were ensured by selecting a useful length of about two times the diameter of the tube. Based on these requirements, the rubber plug initial length was set to 64 mm. The profiles extruded from billet 5 were tested, and, for each profile exit, three different repetitions were performed for a total amount of 9 tests. For each test repetition, the internal rubber plug was changed.

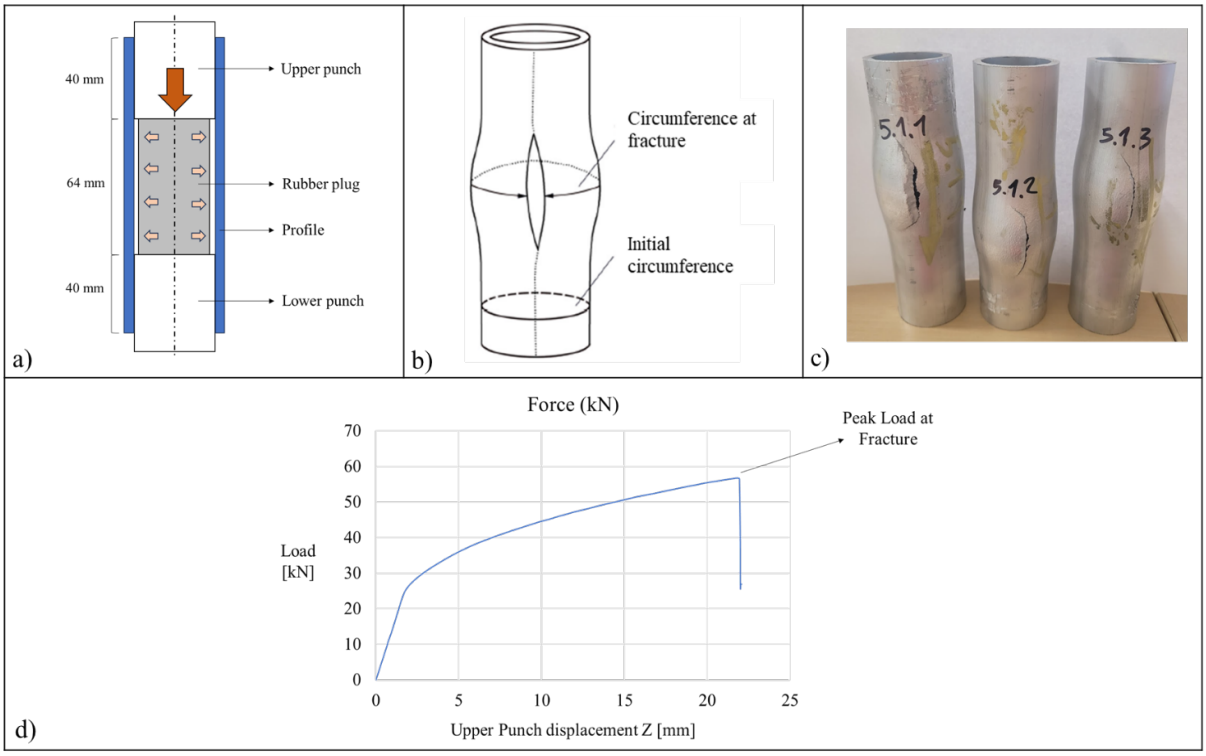

Fig. 15. a) Schematization of the bulge test, b) Initial circumference and circumference at fracture, c) Profiles after the bulge test, d) Force-Upper punch displacement graph.

Fig. 15d shows the typical load–stroke history of a bulge test with a linear behavior between 0 to 2 mm stroke for the upsetting of the plug to internal tube diameter, then from 2 mm the tube expansion is realized up to tube fracture. In Fig. 16, the main outcomes of the analyses are presented for each profile. In Fig. 16a, the hoop strain at fracture is reported, which was estimated as the natural logarithmic ratio between the final and the initial tube circumferences (Fig. 15b). Profile 1, 2 and 3 presented average values of 0.13, 0.08 and 0.14, respectively. In Fig. 16b, the peak load at fracture is shown with average values of 56.1 kN, 51.5 kN and 57.6 kN, respectively. The result of the experimental investigation clearly showed that the profile 3 has the best deformability (both in term of hoop strain and peak load), followed by the profile 1, while the profile 2 presented the lowest values as a consequence of the occurrence of the PCG (coarser grain structure) discussed in the microstructure section. Profile fractures occurred always in the same seam weld (among the three seam welds) within the three repetitions, thus indicating clearly weak welds inside each profile. The identification of the weak seam was not possible since no tracking of the weld orientation was kept on the profiles.

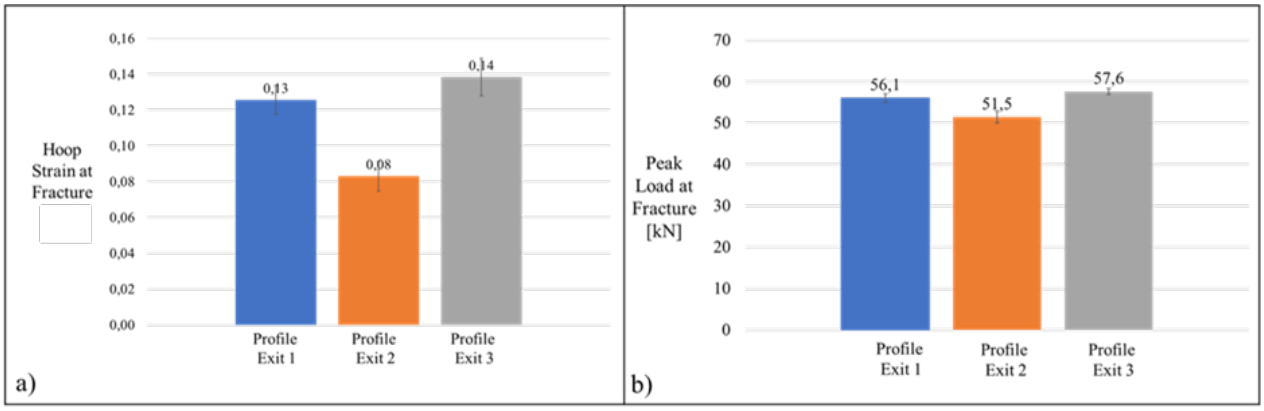

Fig. 16. Results: a) Hoop strain at fracture, b) Peak load at fracture.

Conclusions

In the Extrusion Benchmark 2023, the processing conditions for extruding three AA 6082 tubes were monitored and analyzed. Starting material was tested in terms of flow stress behavior through hot torsion tests, and several input data formats were provided (tabular data, Hansel-Spittel and sin-hyperbolic models). Initial microstructure shape and dimensions were also collected, together with the billet skin thickness. The process was carried out at a constant ram speed of 4,4 mm/s. To guarantee steady state conditions for the analysis of the trials, 15 billets were extruded and the billets 4 and 5 were used for benchmark comparison. During the extrusion, the following process data were acquired in order to provide a reliable comparison of FEM outputs: press load, profile speed, profile temperatures and die temperatures in eleven different locations. Profiles were then analyzed in terms of quality of the seam welds, the microstructure size and the distribution in the profile of charge welds and billet skin evolutions. The analyses were performed on air and water quenched conditions and with the use or absence of liquid nitrogen cooling.

Acknowledgments

Authors would like to strongly acknowledge all the Companies and persons that made possible to carry out the experiment. In particular, the authors acknowledge the operators and the plant director Eng. Luca Gorlani from Metra plant in Rodengo Saiano (BS, italy) for the supply of material and the press usage, and Almax Mori Group (TN, Italy), in particular Eng. Tommaso Pinter, for the die design and manufacturing. All these companies and involved persons are strongly acknowledged for their kind support, activity and problem solving approach.

Funding

National Recovery and Resilience Plan (NRRP), Mission 04 Component 2 Investment 1.5– NextGenerationEU, Call for tender n.3277 dated 30/12/2021 (Award Number: 0001052 dated 23/06/2022).

References

[1] B. Reggiani, L. Donati, L. Tomesani, ICEB - International conference on extrusion and benchmark, Light Metal Age 75 (5) (2017) 52 – 60.

[2] M. Schikorra, L. Donati, L. Tomesani, A. E. Tekkaya, Extrusion Benchmark 2007 – Benchmark Experiments: Study on Material Flow Extrusion of a Flat Die, Key Eng. Mater. 367 (2008)1-8.

[3] D. Pietzka, N. Ben Khalifa, L. Donati, L. Tomesani, A. E. Tekkaya, Extrusion Benchmark 2009 - Experimental analysis of deflection in extrusion dies. Key Eng. Mater. 424 (2010) 19 - 26.

[4] A. Selvaggio, A. Segatori, A. Guzel, L. Donati, L. Tomesani, A. E. Tekkaya, Extrusion Benchmark 2011: Evaluation of different design strategies on process conditions, die deflection and seam weld quality in hollow profiles, Key Eng. Mater. 491 (2012) 1 – 10.

[5] L. Donati. A. Segatori, et al., Effect of liquid nitrogen die cooling on extrusion process conditions Key Eng. Mater. 491 (2012) 215 - 222.

[6] A. Selvaggio, T. Kloppenborg, M. Schwane, et al., Extrusion Benchmark 2013 - Experimental Analysis of Mandrel Deflection, Local Temperature and Pressure in Extrusion Dies, Key Eng. Mater. 585 (2013) 13 – 22.

[7] A. Selvaggio, L. Donati, et al., Scientific Benchmark 2015: Effect of choking and bearing length on metal flow balancing in extrusion dies, Mater. Today: Proc 2 (2015) 4704-4713.

[8] A. Gamberoni, L. Donati, et al., Industrial Benchmark 2015: process monitoring and analysis of hollow EN AW-6063 extruded profile, Mater. Today: Proc 2 (2015) 4714-4725.

[9] L. Donati L., A. Segatori et al., Extrusion Benchmark 2017: Effect of Die Design on Profile Quality and Distortions of Thin C-Shaped Hollow Profiles, Mater. Today: Proc 10 (2019) 171–184.

[10] S. Di Donato, R. Pelaccia, M. Negozio, M. El Mehtedi, B. Reggiani, L. Donati, Hot torsion tests of AA6082 alloy, Key Eng. Mater, under processing in this volume.

[11] A. Hensel, T. Spittel, Kraft- und Arbeitsbedarf bildsamer Formgebungsverfahren, Deutscher Verlag für Grundstoffindustrie: Leipzig, Germany (1978) 336–360.

[12] F. Garofalo, An empirical relation defining the stress dependence of minimum creep rate in metals, Trans. Metall. Soc. AIME 227 (1963) 351-356.

[13] E. Giarmas, D. Tzetzis, Optimization of die design for extrusion of 6xxx series aluminum alloys through finite element analysis: a critical review. Int. J. Adv. Manuf. Technol. 119 (2022) 5529–5551.

[14] L. Donati, B. Reggiani, R. Pelaccia, M. Negozio, S. Di Donato, Advancements in extrusion and drawing: a review of the contributes by the ESAFORM community, Int. J. Mater. Form. 15 (2022) 41.

[15] R. Pelaccia, M. Negozio, S. Di Donato, L. Donati, B. Reggiani, Recent trends in nitrogen cooling modelling of extrusion dies, Key Eng. Mater., under processing in this volume.

[16] B. Reggiani, L. Donati, Comparison of experimental methods to evaluate the seam welds quality in extruded profiles Trans. Nonferrous Met. Soc. China. 30(3) (2020) 619-634.